Evaluation of the antibacterial activity of silver-doped curcumin-loaded zeolitic imidazolate framework-8 against methicillin-sensitive and -resistant *Staphylococcus aureus*

Uroolee Changmai [1, #], Likhith K [1, #], Tarun Mateti [2, #], Malti Kumari [2, #], Savita [2, #], Nagalakshmi Narasimhaswamy [3], Goutam Thakur [1, *]

[1] *Department of Biomedical Engineering, Manipal Institute of Technology, Manipal Academy of Higher Education, Manipal–576104, Udupi, Karnataka, India*

[2] *Materials Research Centre, Indian Institute of Science, Bangalore–560012, Karnataka, India*

[3] *Division of Microbiology, Department of Basic Medical Sciences, Manipal Academy of Higher Education, Manipal–576104, Udupi, Karnataka, India*

[#] **Authors contributed equally**, [*] **Correspondence**: goutam.thakur@manipal.edu

Abstract

Zeolitic imidazolate framework-8 particles (ZIF-8) have attracted attention because of their high drug-loading capabilities. In this study, we synthesized silver (Ag)-doped curcumin (CUR) adsorbed ZIF-8 to test its antibacterial activity against methicillin-sensitive and -resistant *Staphylococcus aureus* (*S. aureus*). Ag-doped curcumin adsorbed ZIF-8 particles (**Ag@CUR/ZIF-8**) were investigated to study their crystallinity, charge, morphology, chemical bonding, absorption, and adsorption characteristics, and the results showed successful loading of curcumin and silver into the ZIF-8 structure. Microstructure analysis using scanning electron microscopy (SEM) revealed that the CUR/ZIF-8 particles have a rhombic dodecahedral morphology and the synthesis of **Ag@CUR/ZIF-8** through doping using Fourier Transform Infrared (FTIR). The nanoparticle size was around 150 nm, while the average crystalline size was 14.768 nm. The minimum inhibitory concentration (MIC) of **Ag@CUR/ZIF-8** was 40 µg/ml against all strains of *S. aureus*, exhibiting substantial antibacterial activity against the pathogens tested. This proves that **Ag@CUR/ZIF-8** displayed superior antibacterial activity through the synergistic effect of CUR, Ag, and zinc ions.

Keywords: zeolitic imidazolate framework-8, silver, curcumin, staphylococcus aureus, antibacterial activity

1. Introduction

Metal-organic frameworks have intrigued researchers worldwide due to their advantageous properties, such as tunable structure, high surface area, and easy chemical functionalization [1]. These are increasingly explored in drug delivery because they possess hydrophobic pockets that encapsulate drugs and chemicals, creating multifunctional theragnostic platforms [2]. Metal-organic frameworks comprise the ZIF-8 subclass, with unique structures and variable chemical surfaces, allowing them to encapsulate molecules within their pores, protect them from degradation, and improve their bioavailability [3]. ZIF-8 comprises zinc ions coordinated with imidazole ligands, forming a three-dimensional porous structure.

Curcumin is the main bioactive compound found in turmeric and has broad-spectrum biological and pharmacological activities [4]; however, its poor bioavailability and low solubility in aqueous mediums limit its therapeutic use [5]. One method of increasing curcumin bioavailability is to use delivery systems [6], which improve its solubility and stability. Moreover, such systems can be functionalized with targeting ligands for site-specific delivery [7].

Silver has been extensively studied for its antibacterial properties against both gram-positive and -negative bacteria [8]; however, it is susceptible to aggregation [9] and potential toxicity [10] without functionalization. Silver could be functionalized by doping it into other nanoparticles, and functionalizing it with organic biomolecules can further enhance its antibacterial properties and reduce potential cytotoxicity.

Although the antibacterial activity of curcumin in ZIF-8 frameworks [11] and Ag-doped ZIF-8 frameworks [12] has been previously studied, the combination of Ag, curcumin, and ZIF-8 has not been investigated yet. In this study, we synthesized Ag-doped curcumin-loaded ZIF-8 frameworks and evaluated their antibacterial activity against methicillin-resistant and -sensitive *Staphylococcus aureus*. The frameworks' morphology, crystallinity, charge, chemical bonding, absorption, and adsorption characteristics were analyzed using suitable characterization techniques.

2. Materials and methods

2.1. Materials

Zinc nitrate hexahydrate, curcumin (CUR), and methanol were purchased from Merck Life Science Pvt. Ltd., India, HiMedia Laboratories Pvt. Ltd., India, and Finar Chemicals, India, respectively. 2-methylimidazole and silver nitrate were purchased from Sigma-Aldrich, India. No further purification of the chemicals was required.

2.2. Synthesis of curcumin-encapsulated ZIF-8 (CUR/ZIF-8)

CUR/ZIF-8 was synthesized by dissolving 1.5 g of zinc nitrate hexahydrate in 50 ml of deionized water and 3.3 g of 2-methylimidazole and 50 mg of curcumin in 100 ml of methanol and mixing and stirring the two solutions for one hour at room temperature. CUR/ZIF-8 was obtained by centrifuging the solution at 13,000 rpm for 30 minutes and washing it with methanol [13].

2.3. Synthesis of Ag-doped-curcumin encapsulated ZIF-8 (Ag@CUR/ZIF-8)

An $AgNO_3$ solution was prepared by mixing 93.75 mg of $AgNO_3$, 2 mL of deionized water, and 20 mL of ethanol and stirring for 15 min. 0.5 g of CUR/ZIF-8 was added to the prepared $AgNO_3$ solution to adsorb Ag^+ ions on its surface, and later, the colloidal solution was centrifuged and washed three times with ethanol and oven dried at 50 ℃ to obtain **Ag@CUR/ZIF-8** [14].

2.4. X-ray diffraction (XRD)

The X-ray diffraction spectrum of CUR, CUR/ZIF-8, and **Ag@CUR/ZIF-8** were recorded using Rigaku Miniflex 600 (5th generation) operating at a voltage of 40 kV and a current of 15 mA between 10–90° at room temperature [15].

2.5. Zeta potential

The zeta potential was measured using a Malvern Zetasizer Nano ZS at a 90° scattering angle. The samples were placed in capillary cells, and measurements were taken in triplicates, with the findings averaged [16].

2.6. Microstructure analysis

The microstructure of CUR/ZIF-8 and **Ag@CUR/ZIF-8** was observed using EVO MA18 with Oxford EDS(X-act) SEM. The samples were vacuum dried, sputtered with gold particles, and examined at various magnifications while exposed to 10 kV voltage [17].

2.7. Functional group analysis

The composition and surface chemistry of CUR/ZIF-8 and **Ag@CUR/ZIF-8** were analyzed using a Shimadzu IRSpirit FTIR spectrometer. A sample pallet was prepared and scanned between 4000–400 cm^{-1} to obtain data on its functional groups and molecular structure [18].

2.8. UV-visible spectroscopy analysis

UV-visible spectroscopy was used to obtain the maximum absorbance wavelength (λ_{max}) of CUR/ZIF-8 and **Ag@CUR/ZIF-8**. Samples were dissolved in methanol to form a homogenous solution, and the absorbance spectra were measured using a LABINDIA analytical UV 3092 spectrophotometer between 200–800 nm [19].

2.9. Brunauer–Emmett–Teller (BET) adsorption analysis

Porosity and surface area were determined using Quantachrome® ASiQwin™ (Quantachrome Instruments, USA). The samples were accurately weighed and degassed for 24 hours at room temperature to achieve a pressure of 2 mHg, and the surface area was calculated using the single-point nitrogen adsorption technique [20].

2.10. Antibacterial activity

The MIC of **Ag@CUR/ZIF-8** was examined against methicillin-sensitive and -resistant *S. aureus* (ATCC 43300; ATCC 25923, ATCC 29213, and MTCC 1430) in a 96-well microtiter plate for 24 h. The *S. aureus* inoculants were made from active bacteria and diluted with Mueller-Hinton broth,

and 100 µL was added to the plate and treated with two-fold dilutions of the **Ag@CUR/ZIF-8** concentrations between 320–0.15 µg/ml. The absorbing value was used to determine the growth of *S. aureus* in the presence of **Ag@CUR/ZIF-8**. The MIC endpoint was declared to be the lowest concentration of **Ag@CUR/ZIF-8**, at which no growth was observed [21].

3. Results and discussion

3.1. X-ray diffraction

Figure 1 shows the crystalline nature of **Ag@CUR/ZIF-8**, CUR/ZIF-8, and CUR, respectively. When comparing the spectrum of CUR/ZIF-8 and CUR, it can be inferred that the periodicity in CUR corresponding to ~9° is altered when it was loaded into ZIF-8 frameworks. Furthermore, the spectrum of **Ag@CUR/ZIF-8** and CUR/ZIF-8 is similar, which reveals that Ag is inert when incorporated within the ZIF-8 frameworks. The crystalline size of the **Ag@CUR/ZIF-8** frameworks was determined to be 14.768 nm using the Scherrer equation (*Supplementary 1*) [22].

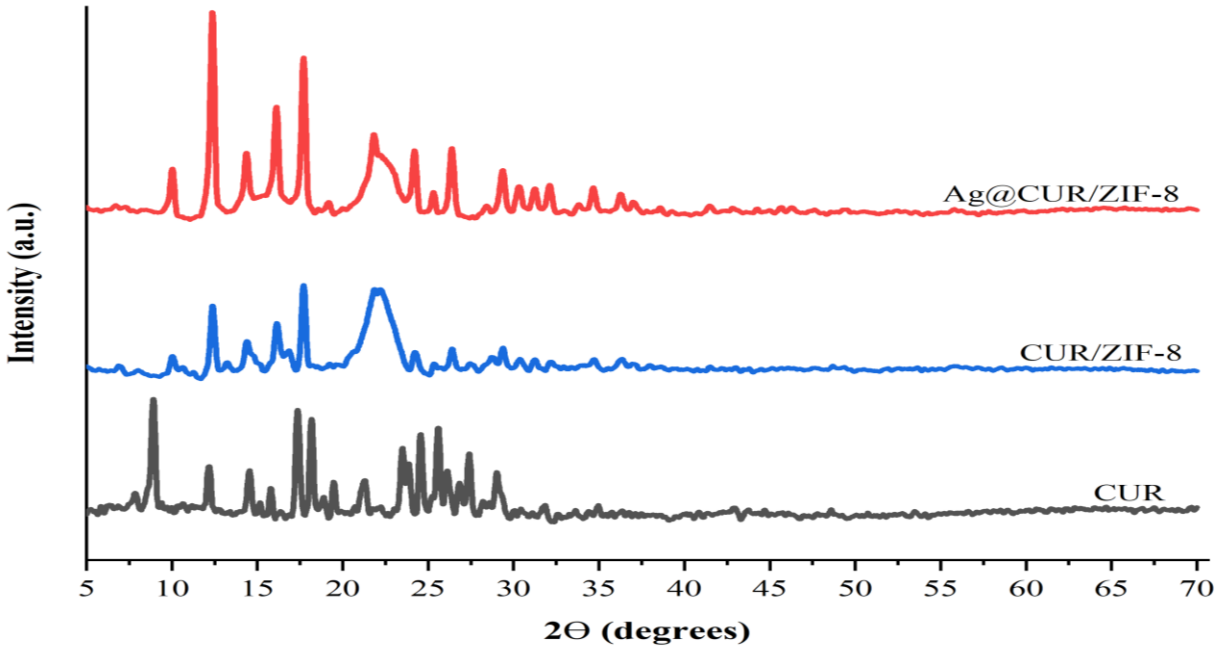

Figure 1. XRD spectra of ***Ag@CUR/ZIF-8****, CUR/ZIF-8, and CUR, respectively.*

3.2. Zeta potential

Figure 2 shows the zeta potential of ZIF-8, CUR/ZIF-8, and **Ag@CUR/ZIF-8**, respectively. It can be inferred that the total charge of both ZIF-8 and CUR/ZIF-8 is negative, while that of **Ag@CUR/ZIF-8** is positive. This is because Ag is a cation, and upon doping it within the CUR/ZIF-8 frameworks, the total charge of the particles became positive.

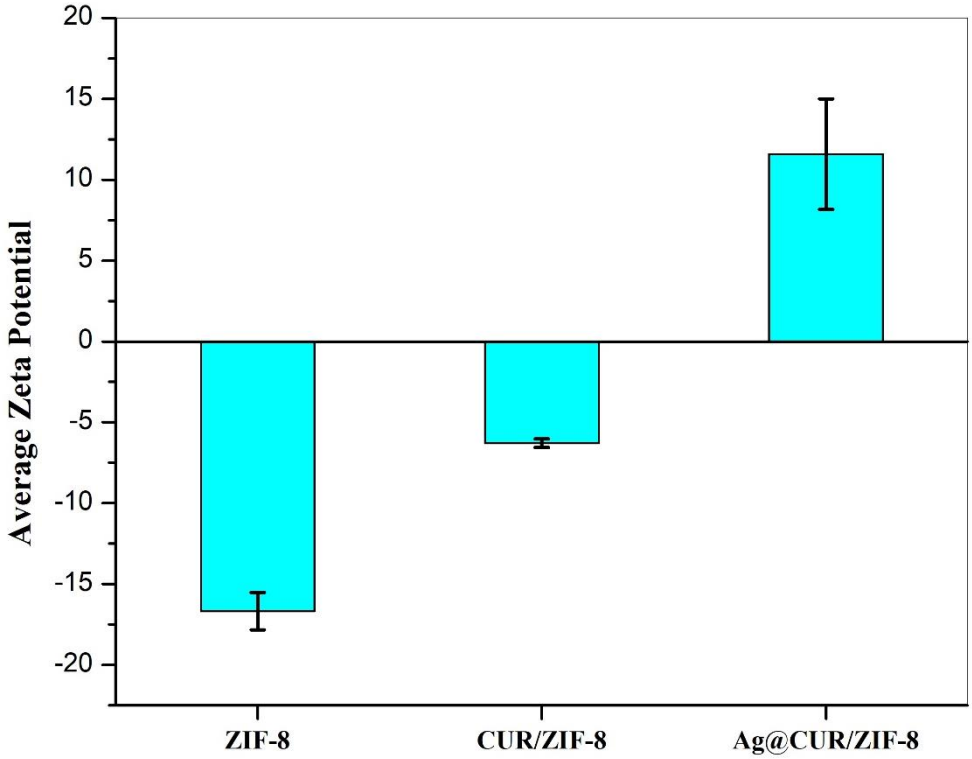

*Figure 2. Zeta potential of ZIF-8, CUR/ZIF-8, and **Ag@CUR/ZIF-8**, respectively.*

3.3. Microstructure analysis

Figure 3 shows the surface microstructure of CUR/ZIF-8 and **Ag@CUR/ZIF-8**, respectively. The SEM micrograph of the CUR/ZIF-8 particles shows that they have a rhombic dodecahedral morphology and are supported by [23], where similar rhombic dodecahedral ZIF-8 particles were obtained. Also, the average diameter of the particles was around 150 nm, which is consistent with [11]. The SEM micrograph of **Ag@CUR/ZIF-8** particles shows the absence of Ag on their exterior surface because Ag is embedded on their interior surface [24]. The **Ag@CUR/ZIF-8** particles appear noticeably rounder and smaller compared to CUR/ZIF-8, as incorporating Ag into the ZIF-8 particles slightly deformed their crystal lattice by binding to the ZIF-8 ligands, resulting in smaller particles [25].

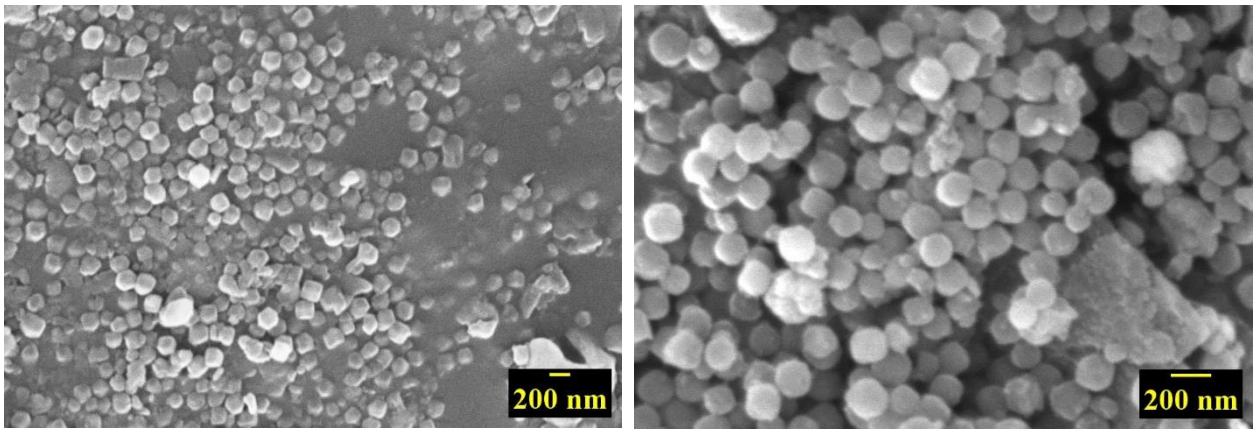

*Figure 3. SEM micrographs of (Left) CUR/ZIF-8 and (Right) **Ag@CUR/ZIF-8**.*

3.4. Functional group analysis

Figure 4 shows the FTIR spectrum of CUR/ZIF-8 and **Ag@CUR/ZIF-8**, respectively. The spectrum of CUR/ZIF-8 shows peaks at 3126 cm^{-1}, 2929 $cm^{-1,}$ and 1588 cm^{-1} corresponding to the aromatic C-H stretching of an imidazole ring, a methyl group, and C-N stretching of imidazole, respectively [26]. The peaks at 1152 cm^{-1}, 1302 cm^{-1}, and 1506 cm^{-1} correspond to the C=C stretching of the C-O-C, C-O, and benzene ring from curcumin, respectively. The phenolic stretching peak of curcumin (*Supplementary 2*) shifted from 3511 cm^{-1} to 3332 cm^{-1}, which implies that curcumin was encapsulated into ZIF-8 [27].

The FTIR spectrum of **Ag@CUR/ZIF-8** contains the primary absorption bands of CUR/ZIF-8 at 3126 cm^{-1}, 2929 cm^{-1}, 1588 cm^{-1}, 1302 cm^{-1} and 1152 cm^{-1}, indicating that Ag unaffected the framework [14]. The wide band at 3488 cm^{-1} shows the stretching vibration of the O-H bond [28].

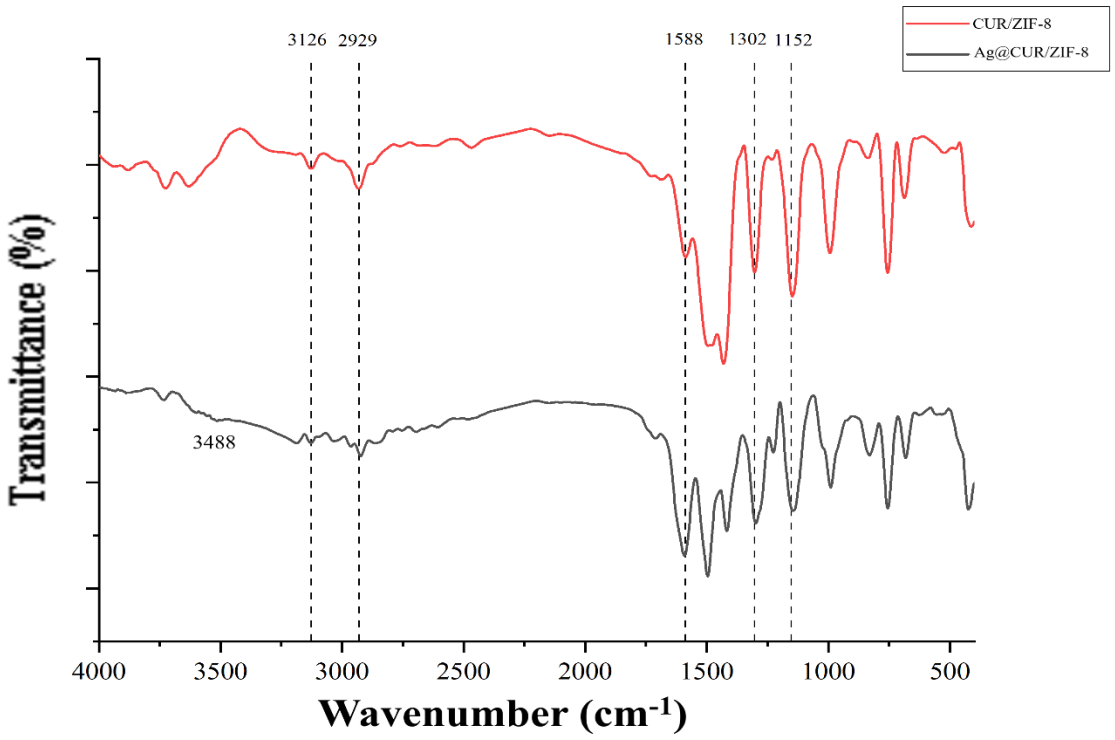

*Figure 4. FTIR spectrum of CUR/ZIF-8 and **Ag@CUR/ZIF-8**, respectively.*

3.5. UV-visible spectroscopy analysis

Figure 5 shows the UV-visible spectrum for **Ag@CUR/ZIF-8** and CUR/ZIF-8, respectively. The CUR/ZIF-8 spectrum has a peak corresponding to curcumin at 453 nm, which is due to the electronic dipole moment that allows π-π* type excitation, while the sharp peak at 218 nm is due to excitonic absorption of the ZIF-8 structure [29], [30]. The **Ag@CUR/ZIF-8** spectrum shows the peaks of ZIF-8 and curcumin, along with an additional broad peak at 320 nm, which could be the absorption band of Ag [31]. The blue shift in the peak of Ag could be due to the formation of ultra-small Ag particles within the ZIF-8 frameworks.

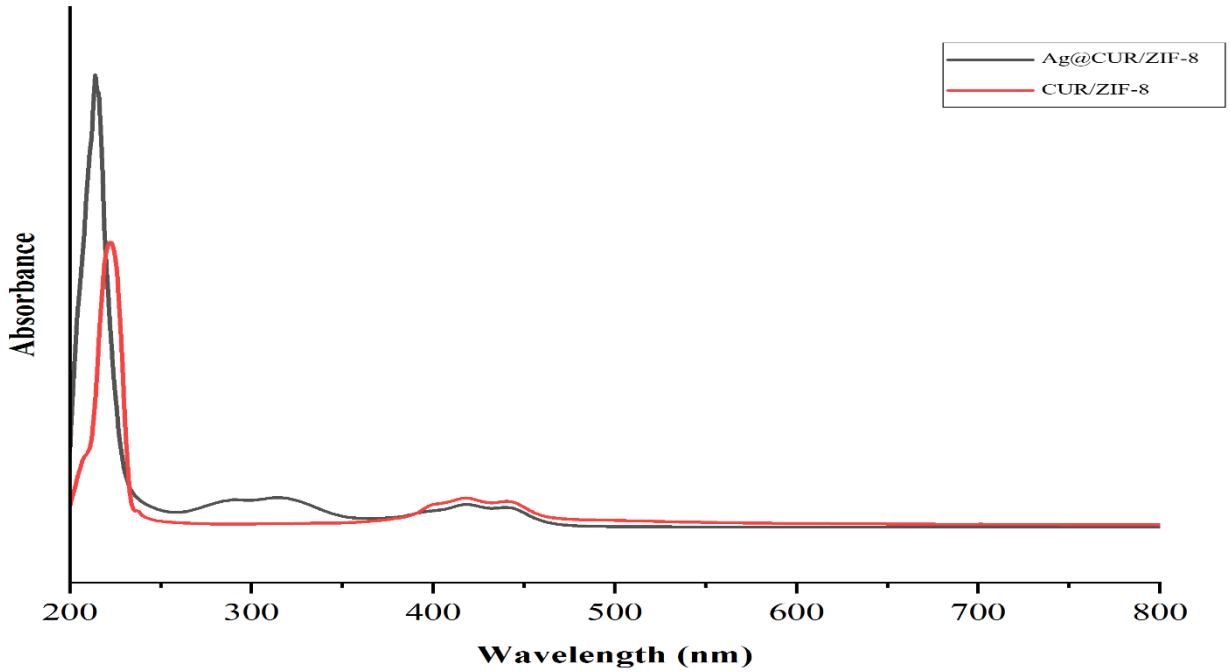

*Figure 5. UV-Visible spectrum of **Ag@CUR/ZIF-8** and CUR/ZIF-8, respectively.*

3.6. BET adsorption analysis

Figure 6 shows the BET porosity and surface area measurements carried out through the nitrogen adsorption–desorption isotherms. It is observed that all of the samples show mesoporous behavior and exhibit a type III isotherm. The pore radius and surface area follow the order: **Ag@CUR/ZIF-8** > CUR/ZIF-8 > ZIF-8, and this indicates that the surface area-to-volume ratio increased upon incorporating Ag into the ZIF-8 frameworks as the particle size became smaller, as depicted in the SEM micrographs.

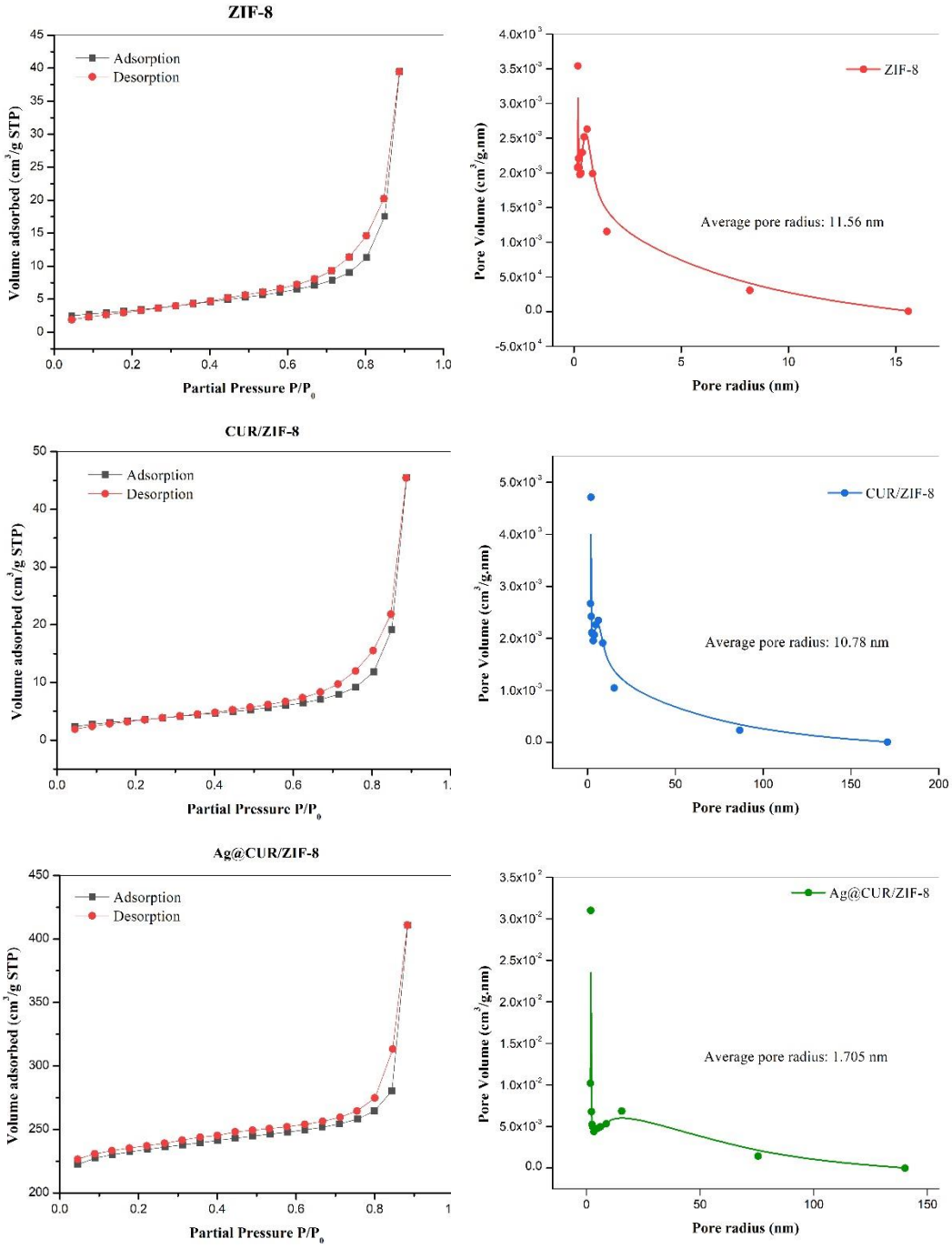

*Figure 6. The adsorption and desorption curves and average pore radius of ZIF-8, CUR/ZIF-8, and **Ag@CUR/ZIF-8**, respectively.*

3.7. Antibacterial activity

Figure 7 shows 96-well microtiter plates containing different strains of *S. aureus* exposed to **Ag@CUR/ZIF-8**. The MIC of **Ag@CUR/ZIF-8** was determined to be 40 µg/ml against all strains. Previously, [11] found that the MIC value of CUR/ZIF-8 against *S. aureus* (ATCC 23235) was 1000 µg/ml, while [12] found the MIC value of **Ag@ZIF-8** against *S. aureus* (ATCC 25922) to be 0.17 mg/ml. Our result shows that **Ag@CUR/ZIF-8** has superior antibacterial activity compared to other studies due to the synergistic effect of curcumin, Ag, and zinc ions [32].

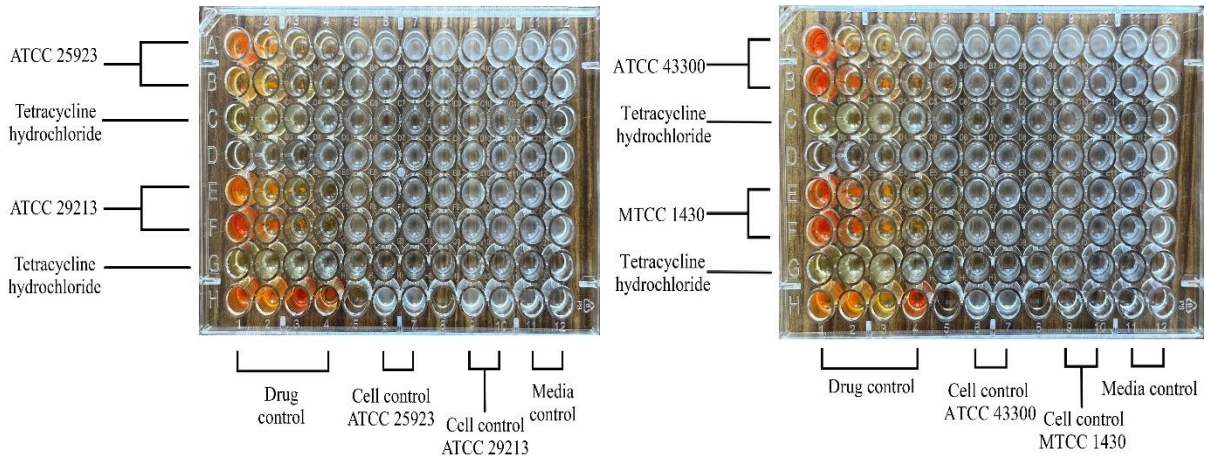

Figure 7. 96-well microtiter plates containing different S. aureus strains exposed to ***Ag@CUR/ZIF-8***

4. Conclusion

This study aimed to develop **Ag@CUR/ZIF-8** to test its antibacterial activity against different strains of *S. aureus*. **Ag@CUR/ZIF-8** particles were synthesized by incorporating ZIF-8 frameworks with CUR and then doping the CUR/ZIF-8 particles with Ag. The SEM micrographs revealed that the CUR/ZIF-8 particles of around 150 nm had a rhombic dodecahedral structure, and incorporating Ag affected their morphology by producing smaller and rounder **Ag@CUR/ZIF-8** particles, whose formation was confirmed by the zeta potential, UV-visible spectroscopy, and FTIR studies. Furthermore, the crystallite size of **Ag@CUR/ZIF-8** was calculated from the XRD graph using the Scherrer equation and was found to be 14.768 nm on average. The antibacterial activity of the **Ag@CUR/ZIF-8** nanoparticles against methicillin-sensitive and -resistant *S. aureus* strains was determined to be 40 µg/ml, indicating the synergistic

antibacterial effect of CUR, Ag, and zinc ions. In conclusion, **Ag@CUR/ZIF-8** particles were found to be superior antibacterial agents for use in drug delivery and biomedical applications.

5. Acknowledgments

The authors would like to acknowledge the Department of Basic Medical Sciences and the Manipal Academy of Higher Education for providing the facility to conduct this research work.

6. Declaration of interests

The authors have no conflicts of interest to declare.

References

[1] H. Furukawa, K. E. Cordova, M. O'Keeffe, and O. M. Yaghi, "The chemistry and applications of metal-organic frameworks," *Science (1979)*, vol. 341, no. 6149, Aug. 2013, doi: 10.1126/SCIENCE.1230444/SUPPL_FILE/FURUKAWA.SM.CORRECTED.PDF.

[2] Y. Zhu *et al.*, "Bioactive MOFs Based Theranostic Agent for Highly Effective Combination of Multimodal Imaging and Chemo-Phototherapy," *Adv Healthc Mater*, vol. 9, no. 14, p. 2000205, Jul. 2020, doi: 10.1002/ADHM.202000205.

[3] S. Feng, X. Zhang, D. Shi, and Z. Wang, "Zeolitic imidazolate framework-8 (ZIF-8) for drug delivery: A critical review," *Front Chem Sci Eng*, vol. 15, no. 2, pp. 221–237, Apr. 2020, doi: 10.1007/S11705-020-1927-8.

[4] S. Mitra, T. Mateti, S. Ramakrishna, and A. Laha, "A Review on Curcumin-Loaded Electrospun Nanofibers and their Application in Modern Medicine," *JOM*, vol. 74, no. 9, pp. 3392–3407, Feb. 2022, doi: 10.1007/S11837-022-05180-9.

[5] A. Shehzad, G. Rehman, and Y. S. Lee, "Curcumin in inflammatory diseases," *BioFactors*, vol. 39, no. 1, pp. 69–77, Jan. 2013, doi: 10.1002/BIOF.1066.

[6] T. Mateti, S. Aswath, A. K. Vatti, A. Kamath, and A. Laha, "A review on allopathic and herbal nanofibrous drug delivery vehicles for cancer treatments," *Biotechnology Reports*, vol. 31, 2021, doi: 10.1016/j.btre.2021.e00663.

[7] F. Jiang *et al.*, "Preparation and protective effects of 1,8-cineole-loaded self-microemulsifying drug delivery system on lipopolysaccharide-induced endothelial injury

in mice," *European Journal of Pharmaceutical Sciences*, vol. 127, pp. 14–23, Jan. 2019, doi: 10.1016/J.EJPS.2018.10.012.

[8] C. Marambio-Jones and E. M. V. Hoek, "A review of the antibacterial effects of silver nanomaterials and potential implications for human health and the environment," *Journal of Nanoparticle Research*, vol. 12, no. 5, pp. 1531–1551, Mar. 2010, doi: 10.1007/S11051-010-9900-Y.

[9] K. S. Pavithra *et al.*, "Polymer-dispersant-stabilized Ag nanofluids for heat transfer applications," *J Therm Anal Calorim*, vol. 146, no. 2, 2021, doi: 10.1007/s10973-020-10064-8.

[10] K. S. Siddiqi, A. Husen, and R. A. K. Rao, "A review on biosynthesis of silver nanoparticles and their biocidal properties," *J Nanobiotechnology*, vol. 16, no. 1, pp. 1–28, Feb. 2018, doi: 10.1186/S12951-018-0334-5.

[11] X. Meng, J. Guan, S. Lai, L. Fang, and J. Su, "pH-responsive curcumin-based nanoscale ZIF-8 combining chemophotodynamic therapy for excellent antibacterial activity," *RSC Adv*, vol. 12, no. 16, pp. 10005–10013, Mar. 2022, doi: 10.1039/D1RA09450E.

[12] Y. Zhang, X. Zhang, J. Song, L. Jin, X. Wang, and C. Quan, "Ag/H-ZIF-8 Nanocomposite as an Effective Antibacterial Agent Against Pathogenic Bacteria," *Nanomaterials*, vol. 9, no. 11, p. 1579, Nov. 2019, doi: 10.3390/NANO9111579.

[13] A. Tiwari, A. Singh, N. Garg, and J. K. Randhawa, "Curcumin encapsulated zeolitic imidazolate frameworks as stimuli responsive drug delivery system and their interaction with biomimetic environment," *Sci Rep*, vol. 7, no. 1, pp. 1–12, 2017.

[14] J. Abdi, "Synthesis of Ag-doped ZIF-8 photocatalyst with excellent performance for dye degradation and antibacterial activity," *Colloids Surf A Physicochem Eng Asp*, vol. 604, p. 125330, Nov. 2020, doi: 10.1016/J.COLSURFA.2020.125330.

[15] M. Azizi-Lalabadi, A. Ehsani, B. Divband, and M. Alizadeh-Sani, "Antimicrobial activity of Titanium dioxide and Zinc oxide nanoparticles supported in 4A zeolite and evaluation the morphological characteristic," *Sci Rep*, vol. 9, no. 1, pp. 1–10, Nov. 2019, doi: 10.1038/s41598-019-54025-0.

[16] Y. Fan, X. Zeng, J. Yi, and Y. Zhang, "Fabrication of pea protein nanoparticles with calcium-induced cross-linking for the stabilization and delivery of antioxidative resveratrol," *Int J Biol Macromol*, vol. 152, pp. 189–198, Jun. 2020, doi: 10.1016/J.IJBIOMAC.2020.02.248.

[17] S. D. Henam, F. Ahmad, M. A. Shah, S. Parveen, and A. H. Wani, "Microwave synthesis of nanoparticles and their antifungal activities," *Spectrochim Acta A Mol Biomol Spectrosc*, vol. 213, pp. 337–341, Apr. 2019, doi: 10.1016/J.SAA.2019.01.071.

[18] M. Paulpandi *et al.*, "Pyrimido quinolin derivative: A potential inhibitor for pandemic influenza A (H1N1) viral growth and its replication," *J Pharm Res*, vol. 6, no. 5, pp. 532–537, May 2013, doi: 10.1016/J.JOPR.2013.04.042.

[19] S. Sathya, V. Ragul, V. P. Veeraraghavan, L. Singh, and M. I. Niyas Ahamed, "An in vitro study on hexavalent chromium [Cr(VI)] remediation using iron oxide nanoparticles based beads," *Environ Nanotechnol Monit Manag*, vol. 14, p. 100333, Dec. 2020, doi: 10.1016/J.ENMM.2020.100333.

[20] K. Reczyńska *et al.*, "Superparamagnetic Iron Oxide Nanoparticles Modified with Silica Layers as Potential Agents for Lung Cancer Treatment," *Nanomaterials*, vol. 10, no. 6, p. 1076, May 2020, doi: 10.3390/NANO10061076.

[21] B. Siddhardha *et al.*, "Chrysin-Loaded Chitosan Nanoparticles Potentiates Antibiofilm Activity against Staphylococcus aureus," *Pathogens*, vol. 9, no. 2, p. 115, Feb. 2020, doi: 10.3390/PATHOGENS9020115.

[22] G. H. Al-Hazmi, A. M. A. Adam, M. G. El-Desouky, A. A. El-Bindary, A. M. Alsuhaibani, and M. S. Refat, "Efficient adsorption of Rhodamine B using a composite of Fe3O4@ zif-8: Synthesis, characterization, modeling analysis, statistical physics and mechanism of interaction," *Bull Chem Soc Ethiop*, vol. 37, no. 1, pp. 211–229, 2023.

[23] M. Zheng, S. Liu, X. Guan, and Z. Xie, "One-Step Synthesis of Nanoscale Zeolitic Imidazolate Frameworks with High Curcumin Loading for Treatment of Cervical Cancer," *ACS Appl Mater Interfaces*, vol. 7, no. 40, pp. 22181–22187, Oct. 2015, doi: 10.1021/ACSAMI.5B04315/ASSET/IMAGES/AM-2015-04315U_M002.GIF.

[24] Q. Bin, M. Wang, and L. Wang, "Ag nanoparticles decorated into metal-organic framework (Ag NPs/ZIF-8) for electrochemical sensing of chloride ion," *Nanotechnology*, vol. 31, no. 12, p. 125601, Jan. 2020, doi: 10.1088/1361-6528/AB5CDE.

[25] N. Chang, Y. R. Chen, F. Xie, Y. P. Liu, and H. T. Wang, "Facile construction of Z-scheme AgCl/Ag-doped-ZIF-8 heterojunction with narrow band gaps for efficient visible-light photocatalysis," *Colloids Surf A Physicochem Eng Asp*, vol. 616, p. 126351, May 2021, doi: 10.1016/J.COLSURFA.2021.126351.

[26] P. Pillai, S. Dharaskar, S. Sasikumar, and M. Khalid, "Zeolitic imidazolate framework-8 nanoparticle: a promising adsorbent for effective fluoride removal from aqueous solution," *Appl Water Sci*, vol. 9, no. 7, pp. 1–12, Oct. 2019, doi: 10.1007/S13201-019-1030-9/FIGURES/13.

[27] A. Tiwari, A. Singh, N. Garg, and J. K. Randhawa, "Curcumin encapsulated zeolitic imidazolate frameworks as stimuli responsive drug delivery system and their interaction with biomimetic environment," *Sci Rep*, vol. 7, no. 1, pp. 1–12, 2017.

[28] R. Mohammadzadeh Kakhki, S. Hedayat, and K. Mohammadzadeh, "Novel, green and low cost synthesis of Ag nanoparticles with superior adsorption and solar based

photocatalytic activity," *Journal of Materials Science: Materials in Electronics*, vol. 30, no. 9, pp. 8788–8795, Apr. 2019, doi: 10.1007/S10854-019-01203-5/FIGURES/9.

[29] B. Kolathupalayam Shanmugam *et al.*, "Curcumin loaded gold nanoparticles–chitosan/sodium alginate nanocomposite for nanotheranostic applications," *J Biomater Sci Polym Ed*, vol. 34, no. 7, pp. 875–892, 2023.

[30] H. Kaur, G. C. Mohanta, V. Gupta, D. Kukkar, and S. Tyagi, "Synthesis and characterization of ZIF-8 nanoparticles for controlled release of 6-mercaptopurine drug," *J Drug Deliv Sci Technol*, vol. 41, pp. 106–112, Oct. 2017, doi: 10.1016/J.JDDST.2017.07.004.

[31] R. M. Tripathi, N. Kumar, A. Shrivastav, P. Singh, and B. R. Shrivastav, "Catalytic activity of biogenic silver nanoparticles synthesized by Ficus panda leaf extract," *J Mol Catal B Enzym*, vol. 96, pp. 75–80, Dec. 2013, doi: 10.1016/J.MOLCATB.2013.06.018.

[32] G. Windiasti *et al.*, "Investigating the synergistic antimicrobial effect of carvacrol and zinc oxide nanoparticles against Campylobacter jejuni," *Food Control*, vol. 96, pp. 39–46, Feb. 2019, doi: 10.1016/J.FOODCONT.2018.08.028.